



HAL
open science

Ligand-Induced Cuboctahedral versus Icosahedral Core Isomerism within Eight-Electron Heterocyclic-Carbene-Protected Gold Nanoclusters

Jianyu Wei, Samia Kahlal, Jean-François Halet, Alvaro Muñoz-Castro,
Jean-Yves Saillard

► **To cite this version:**

Jianyu Wei, Samia Kahlal, Jean-François Halet, Alvaro Muñoz-Castro, Jean-Yves Saillard. Ligand-Induced Cuboctahedral versus Icosahedral Core Isomerism within Eight-Electron Heterocyclic-Carbene-Protected Gold Nanoclusters. *Inorganic Chemistry*, 2022, 61 (23), pp.8623-8628. 10.1021/acs.inorgchem.2c01022 . hal-03716475

HAL Id: hal-03716475

<https://hal.science/hal-03716475>

Submitted on 3 Mar 2023

HAL is a multi-disciplinary open access archive for the deposit and dissemination of scientific research documents, whether they are published or not. The documents may come from teaching and research institutions in France or abroad, or from public or private research centers.

L'archive ouverte pluridisciplinaire **HAL**, est destinée au dépôt et à la diffusion de documents scientifiques de niveau recherche, publiés ou non, émanant des établissements d'enseignement et de recherche français ou étrangers, des laboratoires publics ou privés.

Ligand-induced Cuboctahedral vs. Icosahedral Core Isomerism within 8-electron NHC-protected Gold Nanoclusters

Jianyu Wei,^a Samia Kahlal,^a Jean-François Halet,^{b} Alvaro Muñoz-Castro^{c*} and Jean-Yves Saillard^{a*}*

^aUniv Rennes, CNRS, Institut des Sciences Chimiques de Rennes (ISCR) – UMR 6226, F-35000
Rennes, France.

^bCNRS–Saint-Gobain–NIMS, IRL 3629, Laboratory for Innovative Key Materials and Structures
(LINK), National Institute for Materials Science (NIMS), Tsukuba, 305-0044, Japan.

^cGrupo de Química Inorgánica y Materiales Moleculares, Facultad de Ingeniería, Universidad
Autónoma de Chile, El Llano Subercaseaux 2801, Santiago, Chile.

AUTHOR INFORMATION

Corresponding Author

Jean-François Halet: jean-francois.halet@univ-rennes1.fr

Alvaro Muñoz-Castro: alvaro.munoz@uautonoma.cl

Jean-Yves Saillard: saillard@univ-rennes1.fr

ABSTRACT The controlled structural modification of ligand-protected gold clusters is evaluated by a proper variation of the size and shape of N-heterocyclic carbene (NHC) ligands. DFT calculations show that the Au₁₃ core of [Au₁₃(NHC)₈Br₄]⁺ can be shaped into an icosahedron and/or an unexpected so far cuboctahedron depending on the sterical effect inferred by the NHC ligand side arms. As a result, the cluster properties can be modified, encouraging further exploration on controlled core isomerization in ligated gold cluster chemistry.

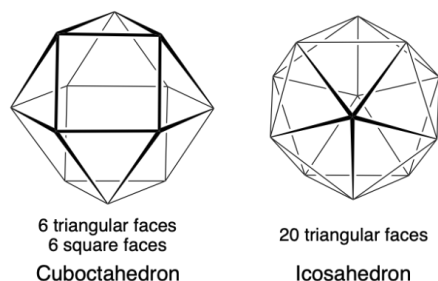
KEYWORDS Gold Nanoclusters; N-heterocyclic Carbene; Superatoms; Core Isomerism

Since the beginning of this century, the field of ligated gold nanoclusters (*AuNCs*) has been the subject of a tremendous development, owing to the many potential applications of these species, associated with their atom-precise nature, allowing accurate chemical control of their properties.¹⁻

³ Such *AuNCs* can be viewed as fully delocalized mixed-valent compounds, with an averaged Au oxidation state comprised between +I and 0 ($5d^{10} 6s^x$ ($0 < x < 1$) average configuration). The bonding in these clusters is associated with the 6s electrons. In the most common cases of clusters having a pseudo-spherical cluster core, the total number of 6s electrons tend to equal a so-called “magic” number (2, 8, 18, 20, 34, 40, 58...), which provides the cluster with closed-shell stability. These specific closed-shell electron counts are rationalized within the concept of *superatom*,⁴⁻⁶ itself derived from the *spherical jellium approximation*⁷ that considers the cluster core as a homogeneous medium in which the electrons in question are subject to a spherical homogeneous potential. It is of critical importance to note that such an approximation assumes that the cluster core should be both spherical and compact enough. The Au@Au₁₂ centered icosahedral arrangement is by far the most pseudo-spherical compact motif encountered in ligated *AuNC* chemistry, as exemplified by the very first *AuNC* characterized by Mingos and colls., namely [Au₁₃(PMe₂Ph)₁₀Cl₂]³⁺,⁸ and the currently extensively studied [Au₂₅(SR)₁₈]⁻ family of compounds, which are described as Au@Au₁₂ centered icosahedra decorated with 18 thiolates and 12 peripheral Au(I) centers.^{9,10} All these compounds can be considered as *superatoms* with an 8-electron [Au₁₃]⁵⁺ core of *I_h* symmetry and 1S² 1P⁶ 1D⁰ *superatomic* configuration. Assuming that these 8 electrons are hosted in molecular orbitals (MOs) expressed as 6s(Au) combinations and using simple 3D Hückel theory, one is lead to a favorable situation in which the bonding *a_g* and *t_{1u}* combinations (1S and 1P within the *spherical jellium approximation*) are occupied, whereas the

antibonding combinations are left vacant. The corresponding total bonding Hückel energy is $|26.96 \beta|$.

Although it can be viewed as a piece of *fcc* bulk, the alternative $M@M_{12}$ centered cuboctahedral arrangement is only slightly less compact than its icosahedral counterpart (Scheme 1). Using again simple 3D Hückel theory for a regular cuboctahedron (O_h symmetry), one is lead to occupied a_{1g} ($1S$) and t_{1u} ($1P$) combinations which are slightly less bonding than their icosahedral counterparts, and consequently the cuboctahedron possesses a slightly lower total bonding Hückel energy of $|24.00 \beta|$. Consistently, the possibility of existence of both cuboctahedral and icosahedral structures for 8-electron clusters has been discussed since a long time.¹¹⁻¹³ In fact, M_{13} centered cuboctahedral *superatoms* exist, as exemplified by the Cu-rich clusters $[(M@Cu_{12})(dithiolate)_6(CCR)_4]^+$ ($M = Cu, Ag, Au$),¹⁴⁻¹⁶ but they are 2-electron *superatoms* ($1S^2 1P^0$). In contrast to copper, all known examples of centered gold clusters with 13 atoms have icosahedral geometries, but a few larger *AuNCs* that contain a distorted Au_{13} cuboctahedral core also exist, as for instance $[Au_{22}(CCR)_{18}]$,^{17,18} $[Au_{40}(SR)_{24}]$,¹⁹ $[AuAg_{28}(SR)_{18}(PPh_3)_4]$,²⁰ and $[Au_{23}(SR)_{16}]^-$.²¹ Only the latter is an 8-electron species.



Scheme 1. Comparative views of the cuboctahedral and icosahedral polyhedra.

It turns out that, within the framework of our general investigations on the stabilization of *AuNCs* by NHCs (NHC = N-heterocyclic carbene),¹²⁻²⁴ we found that some NHCs can, in certain circumstances, stabilize cuboctahedral cluster cores, suggesting rational control of the core

structure with respect to the nature of the ligand shell. NHCs have been recently introduced in *AuNC* chemistry as alternative neutral 2-electron ligands of phosphines and appear to favor promising photo-emissive properties.²⁵⁻³⁸ This is why we recently investigated, by means of density-functional theory (DFT) calculations (see SI for computational details), hypothetical NHC analogues of the 8-electron phosphine/halogenide heteroleptic clusters $[\text{Au}_{13}(\text{PR}_3)_n\text{X}_{12-n}]^{(n-7)+}$ ($X =$ halogen).^{8,39-42} Interestingly, our calculations show that at least in the tetrabromide case, the cuboctahedral $[\text{Au}_{13}(\text{NHC})_8\text{Br}_4]^+$ species can be stabilized, as described below.

Six different NHC ligands of different size and shape were considered, MeIm, EtIm, *i*PrIm, *t*BuIm, *i*PrBzIm and BzBzIm (see top of Figure 1). The assumed starting structure considered in the geometry optimizations is that of the structurally characterized $[\text{Au}_{13}(\text{PR}_3)_8\text{X}_4]^+$ ($X = \text{Cl}, \text{Br}, \text{I}$),^{39,40} *i.e.*, a centered icosahedral core and the four bromide positions describing a tetrahedral-like arrangement. In fact, two bromide ligands are connected to one icosahedral edge and the two others to the opposite vertices of two edge-sharing triangular faces, in such a way that the ideal symmetry of the $\text{Au}_{13}\text{Br}_4$ skeleton is D_{2d} . When the smaller N,N'-dimethylimidazolidene (MeIm) and N,N'-diethylimidazolidene (EtIm) NHC ligands are considered, the centered icosahedral arrangement is conserved (Figure 1). With the medium-sized N,N'-diisopropylimidazolidene (*i*PrIm) ligand, two geometrical isomers fully characterized as true energy minima are found, with an icosahedral and a cuboctahedral core and different orientations of the ligands (Figure 1). The cuboctahedral isomer lies 0.33 eV lower in energy (0.71 eV in free energy) than the icosahedral isomer. This is an interesting result since both isomers are isoelectronic. In general, the icosahedral and cuboctahedral structures differ by their electron count with the latter being more electron-rich than the former. Similar results were also found for the related chloro- and iodo- species $[\text{Au}_{13}(\textit{iPrIm})_8\text{X}_4]^+$ ($X = \text{Cl}, \text{I}$) (Figure S1). With the bulkier ligand N,N'-ditertbutylimidazolidene

(*t*BuIm), two more open-core structures are computed to be stable that can be viewed as highly distorted icosahedral and cuboctahedral arrangements, due to the excessive steric effect of *t*BuIm (Figure 1). The loss of compacity is accompanied by a reduction of the HOMO-LUMO gap (0.85 eV in the most stable cuboctahedral form), suggesting these species are unlikely to be isolated. By replacing the imidazolidine group of *i*PrIm with benzoimidazolidene, a larger sized ligand, N,N'-diisopropylbenzoimidazolidene (*i*PrBzIm), was designed, which led to solely the cuboctahedral structure (Figure 1). Surprisingly, replacing the isopropyl group of *i*PrBzIm with benzyl generates the N,N'-dibenzylbenzoimidazolidene (BzBzIm) ligand, which, despite its still more important size, led to only the icosahedral structure. These results suggest that both the size and shape of the NHC ligands play a crucial role for the icosahedral vs. cuboctahedral core arrangement of $[\text{Au}_{13}(\text{NHC})_8\text{Br}_4]^+$ species, where the use of *i*PrBzIm ensures an effective structural isomerism.

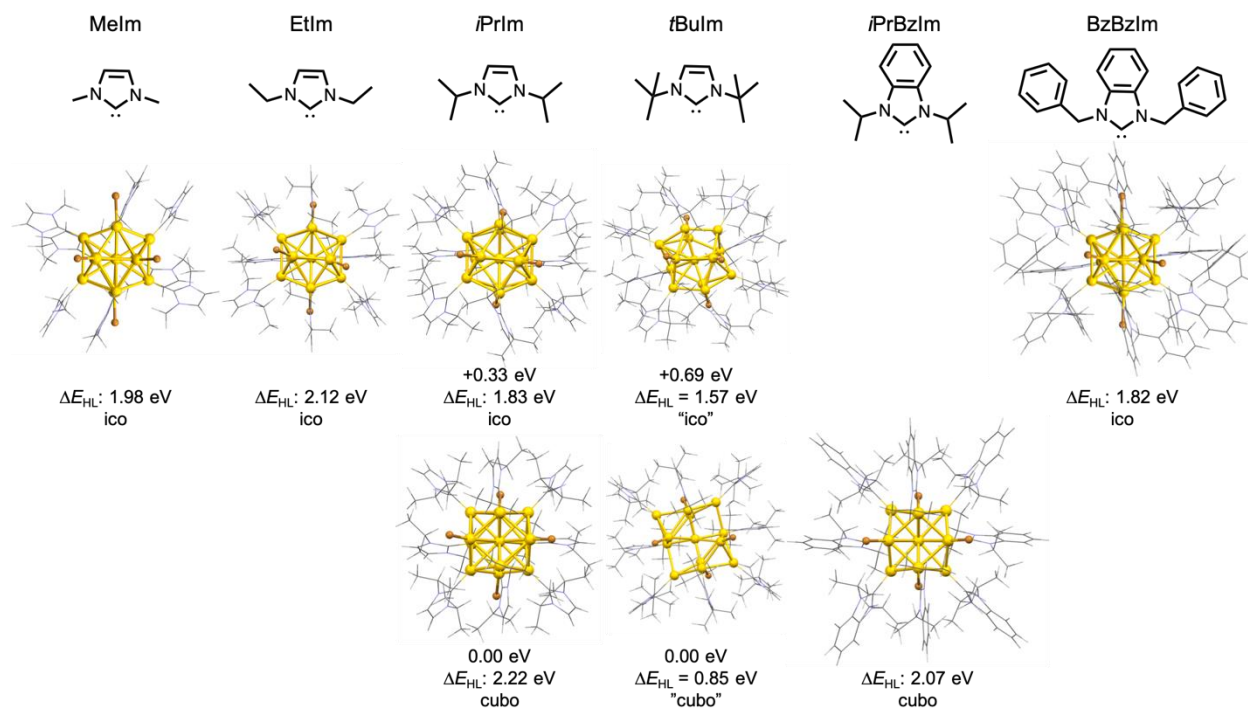


Figure 1. Optimized structures of the investigated $[\text{Au}_{13}(\text{NHC})_8\text{Br}_4]^+$ clusters, with relative energies between isomers. ΔE_{HL} is the HOMO-LUMO gap.

The experimentally characterized phosphine-protected $[\text{Au}_{13}(\text{PMePh}_2)_8\text{Br}_4]^+$ analogue³⁹ was also calculated for comparison (Figure S2). Its optimized structure conserves the experimentally observed icosahedral arrangement and no high-energy cuboctahedral isomer could be found. This gives confidence in the results which were found with the different NHC ligands. To evaluate the steric effect of the phosphine ligands, the larger triphenylphosphine ligand was considered (Figure S2). The optimized structure of $[\text{Au}_{13}(\text{PPh}_3)_8\text{Br}_4]^+$ is comparable to that of the icosahedral species $[\text{Au}_{13}(\text{PMePh}_2)_8\text{Br}_4]^+$. These results indicate that the Au_{13} core isomerization is more likely to occur within NHC-protected species. The Au_{13} core of $[\text{Au}_{13}(\text{PMePh}_2)_8\text{Br}_4]^+$ is more compact than that of the icosahedral form of $[\text{Au}_{13}(i\text{PrIm})_8\text{Br}_4]^+$ (ico), with a shorter average distance between the centered Au and the peripheral Au_{12} shell (Tables S1 and S2).

To further evaluate the influence of the bromide distribution on the Au_{13} core, a model cluster $[\text{Au}_{13}(i\text{PrBzIm})_8\text{Br}_4]^+$ derived from $[\text{Au}_{13}(\text{dppp})_4\text{Cl}_4]^+$,^{41,42} in which the four bromide positions describe a rectangle (ideal symmetry of the $\text{Au}_{13}\text{Br}_4$ skeleton: D_{2h}), was considered. Its optimized structure maintains the icosahedral arrangement (Figure S3), but lies 0.18 eV above the low-energy cuboctahedral isomer.

The Kohn-Sham molecular orbital diagrams of the two isomers of $[\text{Au}_{13}(i\text{PrIm})_8\text{Br}_4]^+$ are shown in Figure 2. They reflect an 8-electron *superatomic* configuration in both cases. In spite of the fact that the $\text{Au}_c\text{-Au}_p$ distances in the icosahedral isomer (av. 2.796 Å) are shorter than those in its cuboctahedral counterpart (av. 2.830 Å), a larger HOMO-LUMO gap is found for the cuboctahedral isomer (Table S1). This counterintuitive result, which is not reproduced in the corresponding bare $[\text{Au}_{13}]^{5+}$ fragments, originates from a ligand effect that tends to lower the energy of the LUMOs of the icosahedral isomer. This effect is to be related to a more important ligand steric congestion in the icosahedral form. Examination of the Au-C bond distances (Table

S4) and of the corresponding Au and C natural atomic orbital (NAO) charges (Table S3) indicate similar metal-ligand bonding in both isomers of $[\text{Au}_{13}(\text{iPrIm})_8\text{Br}_4]^+$.

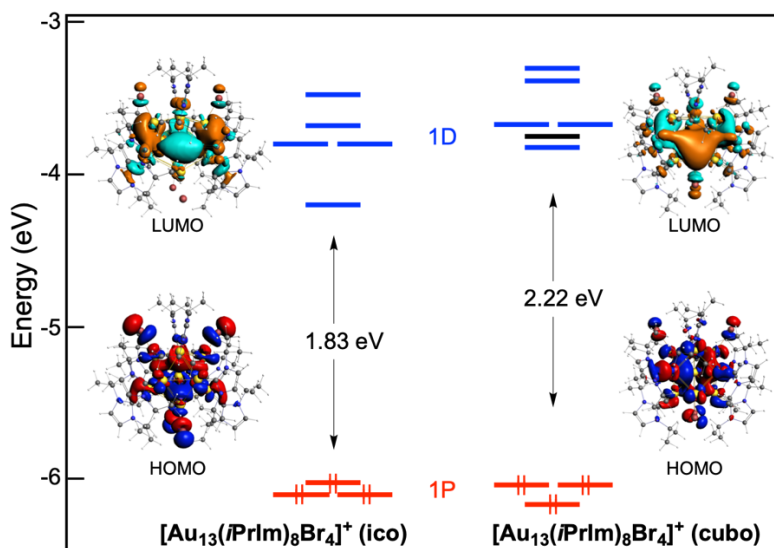


Figure 2. Kohn-Sham molecular orbital diagrams of the $[\text{Au}_{13}(\text{iPrIm})_8\text{Br}_4]^+$ (ico) and $[\text{Au}_{13}(\text{iPrIm})_8\text{Br}_4]^+$ (cubo) isomers. Red, blue and black stick correspond to *superatomic* 1P, 1D and 1F levels, respectively.

The optical properties of both phosphine- and NHC-protected Au_{13} *superatomic* clusters have been widely explored, owing to their potential use as optical devices.^{43,44} It is easily assumed that the tuned kernel structure of a ligated Au_{13} *superatomic* cluster will lead to tailored optical properties. The time-dependent (TD)-DFT simulated UV-Vis spectra of the $[\text{Au}_{13}(\text{NHC})_8\text{Br}_4]^+$ species, as well as that of the experimentally characterized $[\text{Au}_{13}(\text{PMePh}_2)_8\text{Br}_4]^+$ analogue, are gathered in Figure 3a. The shape of the calculated UV-Vis spectra of $[\text{Au}_{13}(\text{PMePh}_2)_8\text{Br}_4]^+$ is in a good agreement with the available experimental spectra.^{39,40} The computed lowest absorption energy wavelength (427 nm) is close to the corresponding experimental value (440 nm). The absorption spectrum of its related NHC counterpart, $[\text{Au}_{13}(\text{iPrIm})_8\text{Br}_4]^+$ (ico), exhibits a red-shifted lowest energy band (518 nm) but a blue-shifted highest energy band, which is in line with our

previous studies.²⁴ As expected, the $[\text{Au}_{13}(\text{iPrIm})_8\text{Br}_4]^+$ (cubo) isomer shows an intrinsically different UV-Vis spectrum. In comparison to its icosahedral isomer, its lowest energy band is blue-shifted to 425 nm, which is in agreement with its larger HOMO-LUMO gap. The absorption spectrum of the cubo-octahedral $[\text{Au}_{13}(\text{iPrBzIm})_8\text{Br}_4]^+$ (cubo) shows similar features as those of $[\text{Au}_{13}(\text{iPrIm})_8\text{Br}_4]^+$ (cubo), suggesting that the differences in the UV-Vis spectra between these $[\text{Au}_{13}(\text{NHC})_8\text{Br}_4]^+$ series are mainly dominated by the Au_{13} core structure, and less affected by the nature of the protecting ligands.

A more detailed analysis of the differences in the optical properties of the icosahedral and cubo-octahedral forms of $[\text{Au}_{13}(\text{iPrIm})_8\text{Br}_4]^+$ can be traced from the MO diagrams shown in Figure 3b. In the case of the icosahedral isomer, the transitions associated to the main absorption band at 518 nm are from the three 1P levels to the $1\text{D}_{x^2-y^2}$ LUMO level. For the cubo-octahedral isomer, the transitions associated to the main absorption band at 425 nm are from two of the three 1P levels (1P_x and 1P_y) to the $1\text{D}_{x^2-y^2}$ type LUMO, 1D_{yz} type LUMO+2 and 1D_{xz} type LUMO+3 levels.

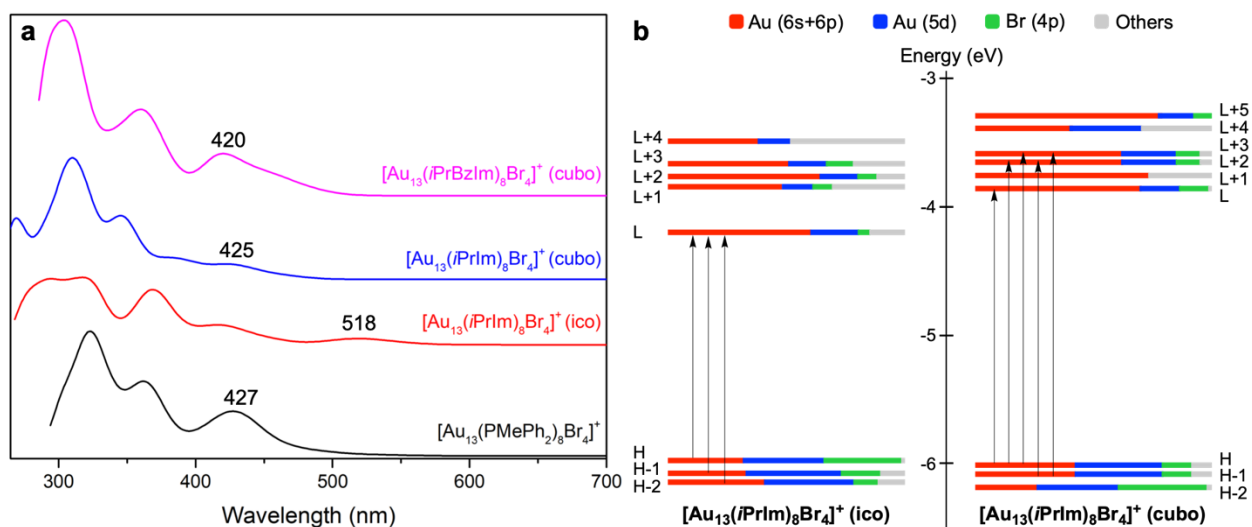


Figure 3. (a) TD-DFT simulated UV-Vis spectra of the $[\text{Au}_{13}(\text{NHC})_8\text{Br}_4]^+$ species as well as the experimentally characterized $[\text{Au}_{13}(\text{PMePh}_2)_8\text{Br}_4]^+$ analogous. (b) The frontier molecular orbitals

composition and the transitions associated to the main absorption band for $[\text{Au}_{13}(\text{iPrIm})_8\text{Br}_4]^+$ (ico) and $[\text{Au}_{13}(\text{iPrIm})_8\text{Br}_4]^+$ (cubo) isomers.

Finally, owing to the relevant photoluminescent properties reported for the experimentally characterized NHC-protected *AuNCs* series²⁵⁻³⁸ ascribed to a phosphorescent emission originating from the $T_1 \rightarrow S_0$ decay, it is also interesting to see the difference in phosphorescent emissions induced by the core isomerization in the investigated $[\text{Au}_{13}(\text{iPrIm})_8\text{Br}_4]^+$ isomers. As for most of the known 8-electron superatoms, the T_1 states of both isomers can be viewed as the result of a HOMO (1P) \rightarrow LUMO (1D) excitation (see Figures S5 and S6). Unsurprisingly, their optimized structures are more expanded than their corresponding S_0 state, the effect being somewhat larger in the case of the cuboctahedral isomer (Table S4 and Figure S4). The phosphorescent emission wavelength of $[\text{Au}_{13}(\text{iPrIm})_8\text{Br}_4]^+$ (ico) is calculated at 1.14 eV (1087 nm), and the value of the $[\text{Au}_{13}(\text{iPrIm})_8\text{Br}_4]^+$ (cubo) isomer is 1.62 eV (765 nm). Such a blue shift of the emission wavelength from the *ico*-isomer to the *cubo*-isomer is in line with the increased HOMO-LUMO gap of the latter one. The low emission energy of the icosahedral form results mainly from the low energy of its S_0 LUMO, due to ligand mixing (see above). These results show that it is possible to design *superatomic* clusters with fine-tuned absorption and emission properties through ligand-induced core isomerization.

In summary, following previous reports on other systems,⁴⁵⁻⁵⁰ we have shown that *AuNC* core isomerization can be ligand-controlled. Our DFT calculations on the hypothetical NHC-protected clusters $[\text{Au}_{13}(\text{NHC})_8\text{X}_4]^+$ ($X = \text{Cl}, \text{Br}, \text{I}$) show that isomerization can be achieved by simply tuning the size and shape of the NHC ligands. When the smaller MeIm and EtIm ligands are considered, the core structure conserves an icosahedral arrangement. With the medium-size *iPrIm* ligand, two isomers with both of icosahedral and (very rare) cuboctahedral core structures are found.

Increasing the ligand size to NHC = *i*PrBzIm leads to the sole cuboctahedral structure. The differences of two $[\text{Au}_{13}(\text{iPrIm})_8\text{Br}_4]^+$ (ico/cubo) isomers in their geometries, electronic structures and optical properties (including emissive properties) were further investigated. In comparison with the icosahedral $[\text{Au}_{13}(\text{iPrIm})_8\text{Br}_4]^+$ isomer, its cuboctahedral variation shows a larger HOMO-LUMO gap, inducing differences in their absorption and emission properties. Our results provide a rational approach to achieve the controllable core isomerization in the widely studied Au_{13} *superatomic* clusters which encourages further exploration on core isomerizations that could induce controlled differences in chemical and physical properties in ligated gold cluster chemistry. Beside of modulating properties through isomerization, the mechanistic isomer interchange pathways, that could be investigated by using variable temperature NMR studies,^{13,51,52} might also deserve interest. The above reported results strongly encourage further experimental work in this direction.

ASSOCIATED CONTENT

Supporting Information Available:

The following files are available free of charge.

Computational details, supplementary optimized geometric structures and computed relevant data. (PDF)

Coordinates of optimized structures. (XYZ)

Notes

The authors declare no competing financial interests.

ACKNOWLEDGMENT

The authors are grateful to the Chilean-French ECOS- CONYCYT Program (Project C18E04) and the French- Chilean International Associated Laboratory for “Multifunctional Molecules and Materials” (LIA-CNRS No. 1027). The GENCI (Grand Equipment National de Calcul Intensif) is acknowledged for HCP support (Project a0010807367). J.W. thanks the China Scholarship Council for a Ph.D. scholarship. A.M.-C. acknowledges support from Fondecyt 1180683 and 1221676.

REFERENCES

- (1) Jin, R.; Zeng, C.; Zhou, M.; Chen, Y. Atomically Precise Colloidal Metal Nanoclusters and Nanoparticles: Fundamentals and Opportunities. *Chem. Rev.* **2016**, *116*, 10346–10413.
- (2) Kang, X.; Li, Y.; Zhu M.; Jin, R. Atomically Precise Alloy Nanoclusters: Syntheses, Structures, and Properties. *Chem. Soc. Rev.* **2020**, *49*, 6443–6514.
- (3) Zhou, M.; Jin, R. Optical Properties and Excited-State Dynamics of Atomically Precise Gold Nanoclusters. *Annu. Rev. Phys. Chem.* **2021**, *72*, 121–142.
- (4) Walter, M.; Akola, J.; Lopez-Acevedo, O.; Jadzinsky, P. D.; Calero, G.; Ackerson, C. J. Whetten, R. L.; Grönbeck, H.; Häkkinen, H. A Unified View of Ligand-protected Gold Clusters as Superatom Complexes. *Proc. Natl. Acad. Sci. USA* **2008**, *105*, 9157–9162.
- (5) Häkkinen, H. Atomic and Electronic Structure of Gold Clusters: Understanding Flakes, Cages and Superatoms from Simple Concepts. *Chem. Soc. Rev.* **2008**, *37*, 1847–1859.
- (6) Jena, P.; Sun, Q. *Superatoms: Principles, Synthesis and Applications*, John Wiley & Sons Ltd, **2022**.
- (7) Knight, W. D.; Clemenger, K.; de Heer, W. A.; Saunders, W. A.; Chou, M. Y.; Cohen, M. L. Electronic Shell Structure and Abundances of Sodium Clusters. *Phys. Rev. Lett.* **1984**, *52*, 2141.

- (8) Briant, C. E.; Theobald, B. R.; White, J. W.; Bell, L. K.; Mingos, D. M. P.; Welch, A. J. Synthesis and X-ray Structural Characterization of The Centred Icosahedral Gold Cluster Compound $[\text{Au}_{13}(\text{PMe}_2\text{Ph})_{10}\text{Cl}_2](\text{PF}_6)_3$; The Realization of a Theoretical Prediction. *J. Chem. Soc. Chem. Commun.* **1981**, 5, 201–202.
- (9) Zhu, M.; Aikens, C. M.; Hollander, F. J.; Schatz, G. C., Jin, R. Correlating the Crystal Structure of A Thiol-Protected Au_{25} Cluster and Optical Properties. *J. Am. Chem. Soc.* **2008**, 130, 5883–5885.
- (10) Kang, X.; Chong, H., Zhu, M. $\text{Au}_{25}(\text{SR})_{18}$: The Captain of The Great Nanocluster Ship. *Nanoscale* **2018**, 10, 10758–10834.
- (11) Mingos, D.M.P. Structural and Bonding Issues in Clusters and Nano-clusters. *Struct. Bond.* **2014**, 162, 1–65.
- (12) Mingos, D.M.P. Structural and bonding patterns in gold clusters. *Dalton Trans.* **2015**, 44, 6680–6695.
- (13) Mingos, D.M.P. Electron Counting Rules for Gold Clusters Which Are Stereochemically Non-rigid and Exhibit Skeletal Isomerism. *Struct. Bond.* **2021**, 188, 1–67.
- (14) Chakrahari, K. K.; Liao, J.-H.; Kahlal, S.; Liu, Y.-C.; Chiang, M.-H.; Saillard, J. -Y.; Liu, C. W. $[\text{Cu}_{13}\{\text{S}_2\text{CN}^m\text{Bu}_2\}_6(\text{acetylide})_4]^+$: A Two-Electron Superatom. *Angew. Chem. Int. Ed.* **2016**, 128, 14924–14928.
- (15) Silalahi, R.P.B.; Chakrahari, K.K.; Liao, J.-H.; Kahlal, S.; Liu, Y.-C.; Chiang, M.H; Saillard, J.-Y.; Liu, C.W. Synthesis of Two-Electron Bimetallic Cu - Ag and Cu - Au Clusters by using $[\text{Cu}_{13}(\text{S}_2\text{CN}^m\text{Bu}_2)_6(\text{C}\equiv\text{CPh})_4]^+$ as a Template. *Chem. Asian J.* **2018**, 13, 500–504.
- (16) Silalahi, R. P. B.; Chiu, T.-H.; Kao, J.-H.; Wu, C.-Y.; Yin, C.-W.; Liu, Y.-C.; Chen, Y. J.; Saillard, J.-Y.; Chiang, M.-H.; Liu, C. W. Synthesis and Luminescence Properties of

Two-Electron Bimetallic Cu–Ag and Cu–Au Nanoclusters via Copper Hydride Precursors. *Inorg. Chem.* **2021**, *60*, 10799–10807.

- (17) Ito, S.; Takano, S.; Tsukuda, T. Alkynyl-Protected $\text{Au}_{22}(\text{C} \equiv \text{CR})_{18}$ Clusters Featuring New Interfacial Motifs and R-Dependent Photoluminescence. *J. Phys. Chem. Lett.* **2019**, *10*, 6892–6896.
- (18) Han, X.; Luan, X.; Su, H.; Li, J.; Yuan, S.; Lei, Z.; Pei, Y.; Wang, Q. M. Structure Determination of Alkynyl-Protected Gold Nanocluster $\text{Au}_{22}(\text{tBuC} \equiv \text{C})_{18}$ and Its Thermochemical Luminescence. *Angew. Chem. Int. Ed.* **2020**, *132*, 2329–2332.
- (19) Zeng, C.; Chen, Y.; Liu, C.; Nobusada, K.; Rosi, N.L.; Jin, R. Gold Tetrahedra Coil up: Kekulé-like and Double Helical Superstructures. *Sci. Adv.* **2015**, *1*, 1500425.
- (20) Kang, X.; Wei, X.; Jin, S.; Yuan, Q.; Luan, X.; Pei, Y.; Wang, S.; Zhu, M.; Jin, R. Rational Construction of a Library of M₂₉ Nanoclusters from Monometallic to Tetrametallic. *Proc. Natl. Acad. Sci. USA* **2019**, *116*, 18834–18840.
- (21) Das, A.; Li, T.; Nobusada, K.; Zeng, C.; Rosi, N.L.; Jin, R. Nonsuperatomic $[\text{Au}_{23}(\text{SC}_6\text{H}_{11})_{16}]^-$ Nanocluster Featuring Bipyramidal Au_{15} Kernel and Trimeric $\text{Au}_3(\text{SR})_4$ Motif. *J. Am. Chem. Soc.* **2013**, *135*, 18264–18267.
- (22) Muñoz-Castro, A. Potential of N-heterocyclic Carbene Derivatives from $\text{Au}_{13}(\text{dppe})_5\text{Cl}_2$ Gold Superatoms. Evaluation of Electronic, Optical and Chiroptical Properties from Relativistic DFT. *Inorg. Chem. Front.* **2019**, *6*, 2349–2358.
- (23) Wei, J.; Halet, J.-F.; Kahlal, S.; Saillard, J.-Y.; Muñoz-Castro, A. Toward the Formation of N-Heterocyclic-Carbene-Protected Gold Clusters of Various Nuclearities. A Comparison with Their Phosphine-Protected Analogues from Density Functional Theory Calculations. *Inorg. Chem.* **2020**, *59*, 15240–15249.
- (24) Wei, J.; Kahlal, S.; Halet, J.-F.; Saillard, J.-Y.; Muñoz-Castro, A. Insight Into the Stability and Electronic and Optical Properties of N-Heterocyclic Carbene Analogues of

Halogen/Phosphine-Protected Au₁₃ Superatomic Clusters. *J. Phys. Chem. A* **2022**, *126*, 536–545.

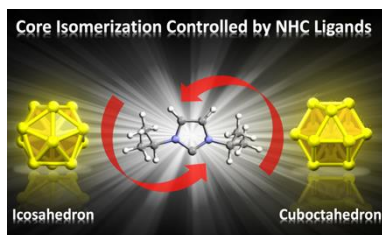
- (25) Ube, H.; Zhang, Q.; Shionoya, M. A Carbon-Centered Hexagold(I) Cluster Supported by N-Heterocyclic Carbene Ligands. *Organometallics* **2018**, *37*, 2007–2009.
- (26) Narouz, M. R.; Osten, K. M.; Unsworth, P. J.; Man, R. W. Y.; Salorinne, K.; Takano, S.; Tomihara, R.; Kaappa, S.; Malola, S.; Dinh, C.-T.; Padmos, J. D.; Ayoo, K.; Garrett, P. J.; Nambo, M.; Horton, J. H.; Sargent, E. H.; Häkkinen, H.; Tsukuda, T.; Crudden, C. M. N-heterocyclic Carbene-functionalized Magic-number Gold Nanoclusters. *Nat. Chem.* **2019**, *11*, 419–425.
- (27) Narouz, M. R.; Takano, S.; Lummis, P. A.; Levchenko, T. I.; Nazemi, A.; Kaappa, S.; Malola, S.; Yousefalizadeh, G.; Calhoun, L. A.; Stamplecoskie, K. G.; Häkkinen, H.; Tsukuda, T.; Crudden, C. M. Robust, Highly Luminescent Au₁₃ Superatoms Protected by N-Heterocyclic Carbenes. *J. Am. Chem. Soc.* **2019**, *141*, 14997–15002.
- (28) Shen, H.; Deng, G.; Kaappa, S.; Tan, T.; Han, Y.; Malola, S.; Lin, S.; Teo, B. K.; Häkkinen, H.; Zheng, N. Highly Robust but Surface-Active: An N-Heterocyclic Carbene-Stabilized Au₂₅ Nanocluster. *Angew. Chem., Int. Ed.* **2019**, *58*, 17731–17735.
- (29) Shen, H.; Xiang, S.; Xu, Z.; Liu, C.; Li, X.; Sun, C.; Lin, S.; Teo, B. K.; Zheng, N. Superatomic Au₁₃ Clusters Ligated by Different N-heterocyclic Carbenes and Their Ligand-dependent Catalysis, Photoluminescence, and Proton Sensitivity. *Nano Res.* **2020**, *13*, 1908–1911.
- (30) Salorinne, K.; Man, R.W.; Lummis, P.A.; Hazer, M.S.A.; Malola, S.; Yim, J.C.H.; Veinot, A.J.; Zhou, W.; Häkkinen, H.; Nambo, M.; Crudden, C.M. Synthesis and Properties of an Au₆ Cluster Supported by a Mixed N-heterocyclic Carbene–thiolate Ligand. *Chem. Commun.* **2020**, *56*, 6102–6105.
- (31) Yi, H.; Osten, K. M.; Levchenko, T. I.; Veinot, A. J.; Aramaki, Y.; Ooi, T.; Nambo, M.; Crudden, C. M. Synthesis and Enantioseparation of Chiral Au₁₃ Nanoclusters Protected by bis-N-heterocyclic Carbene Ligands. *Chem. Sci.* **2021**, *12*, 10436–10440.

- (32) Lei, Z.; Pei, X.; Ube, H.; Shionoya, M. Reconstituting C-Centered Hexagold(I) Clusters with N-Heterocyclic Carbene Ligands. *Bull. Chem. Soc. Jpn.* **2021**, *94*, 1324–1330.
- (33) Hirano, K.; Takano, S.; Tsukuda, T. Ligand Effects on the Structures of $[\text{Au}_{23}\text{L}_6(\text{C}\equiv\text{CPh})_9]^{2+}$ (L = N-Heterocyclic Carbene vs Phosphine) with Au_{17} Superatomic Cores. *J. Phys. Chem. C* **2021**, *125*, 9930–9936.
- (34) Luo, P.; Bai, S.; Wang, X.; Zhao, J.; Yan, Z.; Han, Y.; Zang, S.; Mak, T. C. W. Tuning the Magic Sizes and Optical Properties of Atomically Precise Bidentate N-Heterocyclic Carbene-Protected Gold Nanoclusters via Subtle Change of N-Substituents. *Adv. Opt. Mater.* **2021**, *9*, 2001936.
- (35) Pei, X.; Zhao, P.; Ube, H.; Lei, Z.; Nagata, K.; Ehara, M.; Shionoya, M. Asymmetric Twisting of C-Centered Octahedral Gold(I) Clusters by Chiral N-Heterocyclic Carbene Ligation. *J. Am. Chem. Soc.* **2022**, *144*, 2156–2163.
- (36) Man, R. W. Y.; Yi, H.; Malola, S.; Takano, S.; Tsukuda, T.; Häkkinen, H.; Nambo, M.; Crudden, C. M. Synthesis and Characterization of Enantiopure Chiral Bis NHC-Stabilized Edge-Shared Au_{10} Nanocluster with Unique Prolate Shape. *J. Am. Chem. Soc.* **2022**, *144*, 2056–2061.
- (37) Shen, H.; Tian, G.; Xu, Z.; Wang, L.; Wu, Q.; Zhang, Y.; Teo, B. K.; Zheng, N. N-heterocyclic Carbene Coordinated Metal Nanoparticles and Nanoclusters. *Coord. Chem. Rev.* **2022**, *458*, 214425.
- (38) Hazer, M.S.A.; Malola, S.; Häkkinen, H. Isomer Dynamics of the $[\text{Au}_6(\text{NHC-S})_4]^{2+}$ Nanocluster. *Chem. Commun.* **2022**, *58*, 3218–3221.
- (39) Hall, K. P.; Mingos, D. M. P. Homo- and Heteronuclear Cluster Compounds of Gold. *Prog. Inorg. Chem.* **1984**, *32*, 237–325.
- (40) Copley, R. C. B.; Mingos, D. M. P. Synthesis and Characterization of The Centred Icosahedral Cluster Series $[\text{Au}_9\text{M}^{\text{IB}}_4\text{Cl}_4(\text{PMePh}_2)_8][\text{C}_2\text{B}_9\text{H}_{12}]$, Where $\text{M}^{\text{IB}} = \text{Au}, \text{Ag}$ or Cu . *J. Chem. Soc. Dalt. Trans.* **1996**, *4*, 491–500.

- (41) Shichibu, Y.; Suzuki, K.; Konishi, K. Facile Synthesis and Optical Properties of Magic-number Au₁₃ Clusters. *Nanoscale* **2012**, *4*, 4125–4129.
- (42) Yang, L.; Cheng, H.; Jiang, Y.; Huang, T.; Bao, J.; Sun, Z.; Jiang, Z.; Ma, J.; Sun, F.; Liu, Q.; Yao, T.; Deng, H.; Wang, S.; Zhu, M.; Wei, S. *In situ* Studies on Controlling An Atomically-accurate Formation Process of Gold Nanoclusters. *Nanoscale* **2015**, *7*, 14452–14459.
- (43) Konishi, K. Phosphine-Coordinated Pure-Gold Clusters: Diverse Geometrical Structures and Unique Optical Properties/Responses. *Struct. Bond.* **2014**, *161*, 49–86.
- (44) Konishi, K.; Iwasaki, M.; Shichibu, Y. Phosphine-ligated gold clusters with core+exo geometries: Unique properties and interactions at the ligand–cluster interface. *Acc. Chem. Res.* **2018**, *51*, 3125–3133.
- (45) Chen, Y.; Liu, C.; Tang, Q.; Zeng, C.; Higaki, T.; Das, A.; Jiang, D.; Rosi, N. L.; Jin, R. Isomerism in Au₂₈(SR)₂₀ nanocluster and stable structures. *J. Am. Chem. Soc.* **2016**, *138*, 1482–1485.
- (46) Kang, X.; Huang, L.; Liu, W.; Xiong, L.; Pei, Y.; Sun, Z.; Wang, S.; Wei, S.; Zhu, M. Reversible nanocluster structure transformation between face-centered cubic and icosahedral isomers. *Chem. Sci.* **2019**, *10*, 8685–8693.
- (47) Higaki, T.; Zeng, C.; Chen, Y.; Hussain, E.; Jin, R. Controlling the crystalline phases (FCC, HCP and BCC) of thiolate-protected gold nanoclusters by ligand-based strategies. *CrystEngComm* **2016**, *18*, 6979–6986.
- (48) Weerawardene, K. D. M.; Aikens, C. M. Effect of aliphatic versus aromatic ligands on the structure and optical absorption of Au₂₀(SR)₁₆. *J. Phys. Chem. C* **2016**, *120*, 8354–8363.
- (49) Tang, Q.; Ouyang, R.; Tian, Z.; Jiang, D. The ligand effect on the isomer stability of Au₂₄(SR)₂₀ clusters. *Nanoscale* **2015**, *7*, 2225–2229.

- (50) Nasaruddin, R. R.; Chen, T.; Yan, N.; Xie, J. Roles of thiolate ligands in the synthesis, properties and catalytic application of gold nanoclusters. *Coord. Chem. Rev.* **2018**, *368*, 60–79.
- (51) Briant, C. E.; Hall, K. P.; Mingos, D. M. P. Structural characterisation of two crystalline modifications of $[\text{Au}_9\{\text{P}(\text{C}_6\text{H}_4\text{OMe-}p)_3\}_8](\text{NO}_3)_3$: the first example of skeletal isomerism in metal cluster chemistry. *J. Chem. Soc., Chem. Commun.* **1984**, 290–291.
- (52) Mingos, D. M. P.; Watson, M. J. Recent developments in the homo- and hetero-metallic cluster compounds of gold. *Transition Met. Chem.* **1991**, *16*, 285–287.

TOC GRAPHICS



The ligand size and shape allow controlling the core structure and associated properties